Si nanowire phototransistors at telecommunication wavelengths by plasmon-enhanced two-photon absorption

Hamidreza Siampour and Yaping Dan*

State Key Laboratory of Advanced Optical Communication Systems and Networks, University of Michigan-Shanghai Jiao Tong University Joint Institute, Shanghai Jiao Tong University, Shanghai, 200240, China
yaping.dan@sjtu.edu.cn

Abstract: The on-chip integration of optical waveguides with complementary metal-oxide-semiconductor (CMOS) transistors is the next generation technology for high-speed communications. The advance of such a technology requires a high-performance photodetector operating at communication wavelengths. However, silicon does not absorb photons at communication wavelengths because of its relatively large bandgap. Growing high quality small bandgap semiconductors on top of silicon is challenging due to lattice mismatch. An all silicon photonic CMOS technology is an attractive option. Here, we demonstrate a high-performance silicon phototransistor that operates at the communication wavelengths by two-photon absorption effect. To turn silicon into a light absorptive material at communication wavelengths, we have designed a sophisticated plasmonic antenna structure to increases the intensity of light in the silicon nanowire by 5 orders of magnitude. At the high light intensity, the light absorption in silicon is dominated by the two-photon absorption effect. The generated photocurrent is further amplified by the Si nanowire phototransistor, a section of which is doped to be a core-shell pn junction. Simulation results indicate that the device can achieve a responsivity of 2.4×10^4 A/W and a 3-dB bandwidth over 300 GHz. Successful development of such a device is important for the next generation high-speed communication technology.

OCIS codes: (040.5160) Photodetectors; (060.0060) Fiber optics and optical communications; (190.0190) Nonlinear optics; (250.5403) Plasmonics; (250.5300) Photonic integrated circuits.

References and links

1. M. Haurylau, G. Chen, H. Chen, J. Zhang, N. A. Nelson, D. H. Albonesi, E. G. Friedman, and P. M. Fauchet, "On-Chip Optical Interconnect Roadmap: Challenges and Critical Directions," IEEE J. Sel. Top. Quantum Electron. **12**(6), 1699–1705 (2006).
2. G. Chen, H. Chen, M. Haurylau, N. A. Nelson, D. H. Albonesi, P. M. Fauchet, and E. G. Friedman, "Predictions of CMOS compatible on-chip optical interconnect," Integration **40**(4), 434–446 (2007).
3. G. Roelkens, L. Liu, D. Liang, R. Jones, A. Fang, B. Koch, and J. Bowers, "III-V/silicon photonics for on-chip and intra-chip optical interconnects," Laser Photonics Rev. **4**(6), 751–779 (2010).
4. L. Tang, S. E. Kocabas, S. Latif, A. K. Okyay, D. S. Ly-Gagnon, K. C. Saraswat, and D. A. B. Miller, "Nanometre-scale germanium photodetector enhanced by a near-infrared dipole antenna," Nat. Photonics **2**(4), 226–229 (2008).
5. J. Michel, J. Liu, and L. C. Kimerling, "High-performance Ge-on-Si photodetectors," Nat. Photonics **4**(8), 527–534 (2010).
6. B. Jalali, "Silicon photonics: Nonlinear optics in the mid-infrared," Nat. Photonics **4**(8), 506–508 (2010).
7. M. Casalino, G. Coppola, M. Iodice, I. Rendina, and L. Sirleto, "Near-infrared sub-bandgap all-silicon photodetectors: state of the art and perspectives," Sensors (Basel) **10**(12), 10571–10600 (2010).
8. R. Dekker, N. Usechak, M. Först, and A. Driessen, "Ultrafast nonlinear all-optical processes in silicon-on-insulator waveguides," J. Phys. D Appl. Phys. **40**(14), R249–R271 (2007).

#255137 Received 4 Dec 2015; revised 13 Feb 2016; accepted 13 Feb 2016; published 24 Feb 2016

9. A. D. Bristow, N. Rotenberg, and H. M. van Driel, "Two-photon absorption and Kerr coefficients of silicon for 850–2200nm," Appl. Phys. Lett. **90**(19), 191104 (2007).
10. L.-D. Haret, X. Checoury, Z. Han, P. Boucaud, S. Combrié, and A. De Rossi, "All-silicon photonic crystal photoconductor on silicon-on-insulator at telecom wavelength," Opt. Express **18**(23), 23965–23972 (2010).
11. H. Raether, Surface Plasmons on Smooth and Rough Surfaces and on Gratings. Springer (1988).
12. T. Ishi, J. Fujikata, K. Makita, T. Baba, and K. Ohashi, "Si nano-photodiode with a surface plasmon antenna," Jpn. J. Appl. Phys. **44**(12 3L), L364–L366 (2005).
13. D. Wang, T. Yang, and K. B. Crozier, "Optical antennas integrated with concentric ring gratings: electric field enhancement and directional radiation," Opt. Express **19**(3), 2148–2157 (2011).
14. X. He, L. Yang, and T. Yang, "Optical nanofocusing by tapering coupled photonic-plasmonic waveguides," Opt. Express **19**(14), 12865–12872 (2011).
15. N. C. Lindquist, P. Nagpal, K. M. McPeak, D. J. Norris, and S. H. Oh, "Engineering metallic nanostructures for plasmonics and nanophotonics," Rep. Prog. Phys. **75**(3), 036501 (2012).
16. J. Kalbacova, R. D. Rodriguez, V. Desale, M. Schneider, I. Amin, R. Jordan, and D. R. T. Zahn, "Chemical stability of plasmon-active silver tips for tip-enhanced Raman spectroscopy," Nanospectroscopy **1**(1), 12–18 (2015).
17. M. S. Ünlü, B. B. Goldberg, W. D. Herzog, D. Sun, and E. Towe, "Near-field optical beam induced current measurements on heterostructures," Appl. Phys. Lett. **67**(13), 1862–1864 (1995).
18. J. D. Christesen, X. Zhang, C. W. Pinion, T. A. Celano, C. J. Flynn, and J. F. Cahoon, "Design principles for photovoltaic devices based on Si nanowires with axial or radial p-n junctions," Nano Lett. **12**(11), 6024–6029 (2012).
19. S. L. Tan, X. Zhao, and Y. Dan, "High-sensitivity silicon nanowire phototransistors," Proc. SPIE **9170**, 917002 (2014).
20. S. Donati, *Photodetectors* (Prentice Hall PTR, 1999).

1. Introduction

The development of complementary metal-oxide-semiconductor (CMOS) technology has generated a huge impact on our society by offering high-performance electronics at low cost. This is realized by constantly scaling down the size of CMOS transistors, which speeds up the transistors but unfortunately increases the time delay of metal interconnects [1,2]. The operating frequency of modern integrated circuitry is increasingly limited by the delay of metal interconnects instead of CMOS transistors [2]. One promising solution is to replace the metal interconnects, particularly the metal buses, with on-chip optical waveguides, turning the CMOS circuitry into a mixed optical and electronic system. The advance of such a technology requires integrating high-performance photodetectors with CMOS transistors for optical and electronic signal conversion. However, the long haul optical fiber communication uses light at wavelength of 1.31 μm or 1.55 μm, which is below the absorption edge of silicon. Decades of research efforts have been devoted to the heterogeneous growth of small bandgap semi-conductors on top of silicon for photodetection at communication wavelengths [3]. Unfortunately, these efforts are not well paid off due to the unsolved issues such as lattice mismatch which seriously degrades the device performance, although progress has been made recently in SiGe synthesis [4,5]. Efforts on sub-bandgap detection for all-silicon photo-detectors have also been pursued in the past decades by exploring optical absorption *via* mid-bandgap defects, surface-states or internal photo-emission [6,7].

Here, we propose to develop high-performance all silicon photodetectors at communication wavelengths by utilizing two-photon absorption (TPA), a nonlinear effect that allows two coherent photons absorbed simultaneously to generate one electron-hole pair [6,7]. The TPA effect is normally negligible but can become significant at high light intensity. Surface-plasmon antennas are employed to enhance the light intensity in the Si nanowire (SiNW) by orders of magnitude. The photocurrent generated by TPA can be further amplified by turning the nanowire into a core-shell phototransistor. Our simulation results indicate that the responsivity of the silicon nanowire phototransistor at 1.31μm is ~10^4 A/W and the 3-dB bandwidth reaches a record of over 300 GHz.

2. Principles

Silicon has a bandgap of 1.12 eV. For light longer than 1.1μm in wavelength (the absorption edge of silicon), the absorption by silicon will dramatically reduce. For example, the

#255137 Received 4 Dec 2015; revised 13 Feb 2016; accepted 13 Feb 2016; published 24 Feb 2016

absorption coefficient near the two communication wavelengths 1.31 μm and 1.55 μm is approximately 5 and 10 orders of magnitude smaller than that at 1.1μm, respectively. Silicon is therefore photo insensitive at the communication wavelengths. The TPA effect is a nonlinear phenomenon that allows two coherent photons to be absorbed simultaneously [6,7]. This effect may become significant at certain condition. We explore the possibility of turning silicon to be a photo-sensitive material at the communication wavelengths by taking the advantage of the TPA effect.

As known, the absorption coefficient is expressed in Eq. (1) when the TPA effect is included:

$$\alpha(I) = \alpha_0(\lambda) + \beta \times I \tag{1}$$

where α_0 is the one photon absorption coefficient which is wavelength (λ) dependent, I the light intensity, and β the TPA coefficient [8]. For silicon, it is experimentally found that $\beta = 1.7 \times 10^{-9}$ cm/W is a constant independent of wavelength near the telecom band [9].

Note that the light intensity after passing through a semiconductor of a thickness of z follows

$$I = I_0 e^{-\alpha(I)z} \tag{2}$$

Light intensity loss due to the absorption by a semiconductor with a small thickness of Δz is expressed as

$$\Delta \mathrm{I} = \left|\frac{dI}{dz}\right| \Delta z = I \cdot \alpha(I) \cdot \Delta z \tag{3}$$

By plugging Eq. (1) into Eq. (3), we find

$$\Delta \mathrm{I} = \alpha_0(\lambda) \cdot I \cdot \Delta z + \beta \cdot I^2 \cdot \Delta z \tag{4}$$

The first term on the right side of Eq. (4) is due to the one photon absorption, which will rapidly drop at longer wavelengths. The second term accounts for the light absorption by the TPA effect which is proportional to the square of light intensity and independent of wavelength. Clearly, light absorption by the TPA effect will quickly ramp up as the light intensity increases. As a result, the TPA effect may become dominant for long wavelengths in particular. Previously, micro and nano sized photonic crystals were employed to enhance the light intensity for TPA effect in silicon. A performance of 20 mA/W in responsivity and 1 GHz in bandwidth has been achieved for the silicon photodetector at the communication wavelengths [10]. We believe that plasmonic antennas are more suitable for this application than photonic crystals. Plasmonic antennas can enhance the light intensity orders of magnitude by confining light into a nanosized region, as a result of which the TPA effect will be strong. It is known that nanosized photodetectors can achieve high speed but often suffer from low photosensitivity due to the ultra-scaled volume for light absorption. Nanoscale photodetectors integrated with plasmonic antennas can overcome this issue to achieve high speed and high photosensitivity.

3. Design of plasmonic antennas and SiNW photodetectors

The plasmonic antenna structure that we designed to enhance light intensity consists of three components: concentric gratings, fan-rods and tapered dipoles, as shown in Fig. 1. The fan-rods and concentric gratings are made of a continuous Ag film on top of silicon nanoribbons that are formed by patterning the device layer of an SOI wafer. Conveniently, they also serve as the electrodes for the silicon nanowire (SiNW) photodetector which is located at the center.

#255137 Received 4 Dec 2015; revised 13 Feb 2016; accepted 13 Feb 2016; published 24 Feb 2016

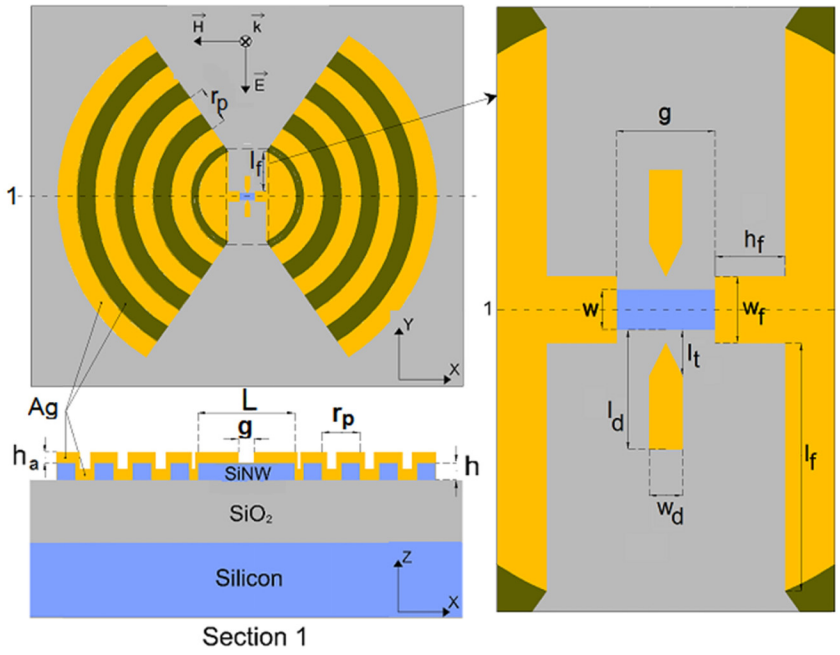

Fig. 1. Plasmonic antenna structure. 3-dimensional (3D) finite difference time domain (FDTD) simulations are performed using the FDTD module of Lumerical. Plane wave is launched perpendicularly from the top, as indicated by the propagation vector $\vec{k}$. r_p is the period of the concentric grating rings. g and w are the length and width of the nanogap, respectively. l_d and W_d are the length and width of the tapered dipole arm, respectively, and l_t is the tapered length. l_f is the radius of the fan-rod antenna, and h_f and W_f are the corresponding rod's length and width, respectively. h and h_a are the thickness of the silicon and metal (silver) layers, respectively. L is the length of the SiNW. Top-left: top view. Bottom-left: cross-section cut along the line "1". Right: close-up view of the center.

The tapered dipoles are perpendicularly across the SiNW. All the three components are designed to resonate at the telecommunication window of 1310 nm, creating "hotspots" in SiNW and therefore an absorption peak around this wavelength as shown in Fig. 2. The design principle is discussed as following. Note that the effective refractive index of the Si/Ag is estimated to be 3.64 [11,12]. To allow the concentric grating to resonate at, for example, around 1310 nm, the grating period r_p shall be equal to the effective resonance wavelength of ~360 nm (= 1310nm/3.64). The purpose of the concentric gratings is to guide the surface plasmon resonances to the center where the fan-rod antennas are located. The propagating plasmon resonances are coupled into the fan-rod antennas that are also designed to resonate at 1310 nm based on the principle described in [13]. The coupling allows for an increase of 2 orders of magnitude in light intensity that enhances the Si nanowire absorption cross section (ACS) up to −160 dBsm as shown in the inset of Fig. 2(c) (black line). The tapered dipole operating as a half-wave dipole further concentrates the plasmon resonances to a deep sub-wavelength region [4,14], enhancing the light intensity another 3 orders of magnitude to approximately −130 dBsm in ACS (red line in the inset of Fig. 2(c)), as a result of which "hotspots" in the Si nanowire are created (Figs. 2(a) and 2(b)). According to Eq. (4), an increase of 5 orders of magnitude in light intensity allows the TPA effect to contribute ~ 90 percent of the total absorption. This is equivalent to silicon becoming 10 times more

#255137 Received 4 Dec 2015; revised 13 Feb 2016; accepted 13 Feb 2016; published 24 Feb 2016

absorptive at 1310nm than at the absorption edge (1100nm) without light intensity enhancement. The resultant TPA cross section of the Si nanowire is shown in Fig. 2(c).

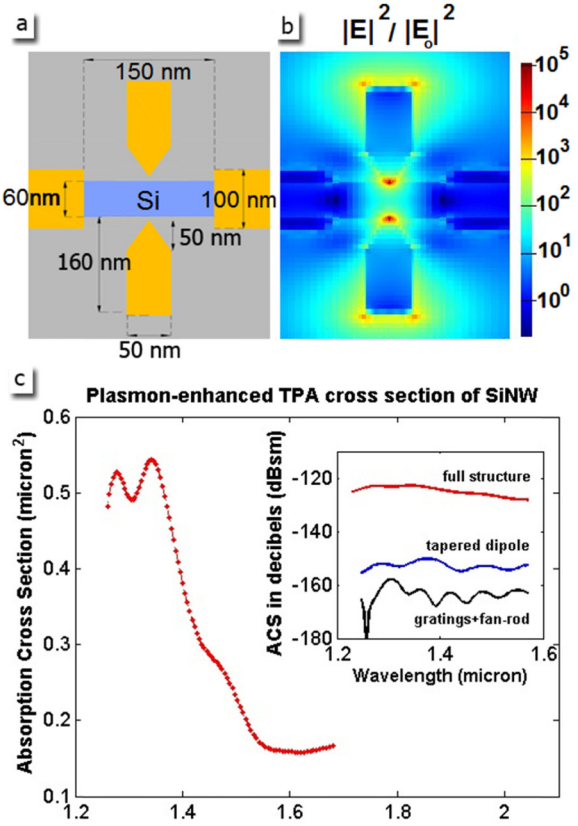

Fig. 2. (a) Geometrical parameters of the nanowire detector; (b) Distribution of normalized light intensity $\left|\vec{E}\right|^2 / \left|\overrightarrow{E_0}\right|^2$ at the half thickness of the nanowire, where $\overrightarrow{E_0}$ is the electric field intensity of the incident light; (c) Absorption cross section (ACS) of the silicon nanowire after the enhancement. The resonant absorption peak is around 1310 nm in wavelength which is applicable for optical communications. Inset: ACS in decibels by coupling grating rings and fan-rod (black line), tapered dipole without gratings and fan-rod (blue line), and full structure of plasmonic antenna including grating rings, fan-rod and tapered dipole (red line).

The sharp tip of the tapered dipole helps enhance the light intensity. But Ag sharp tips at deep nanometer scale are not thermally stable [15,16], even if the fabrication is successful. We replace the tapered diople with a pair of rectangular dipoles and estimate the impact on the device performance. It turns out that the impact is limited (see Figs. S1 and S2 in the supplementary materials). The geometrical parameters of the plasmonic antennas integrated with the SiNW photodetector are listed in Table 1. The SiNW in the nanogap has a short length of $g = 150\,nm$, which helps improve the high-speed performance of the device. Furthermore, the localized interaction between surface plasmon resonances and the small Si region provides a high responsivity for the detector [12,17]. The polarization of the illuminated light is chosen to be parallel to the dipole arms (Fig. 1).

To convert the light absorption into photocurrent, the Si nanowire is normally made into a pn junction photodiode under reverse bias. The simulation results indicate that such a device only generates a negligibly small photocurrent (~20 pA, mainly due to TPA) under a relatively strong incident light intensity of $1 Wcm^{-2}$, even though the light intensity in the

#255137 Received 4 Dec 2015; revised 13 Feb 2016; accepted 13 Feb 2016; published 24 Feb 2016

silicon nanowire has been enhanced 5 orders of magnitude by the plasmon antennas. Electrical amplification of another 3-5 orders of magnitude is needed to reach a photocurrent of tens of

Table 1. Geometrical parameters of the plasmonic antennas integrated with Si nanowire detecto

Element	Planar structure	Parameters (nm)	Thickness (nm)
SiNW	rectangle	$L = 880$ $w = 60$	80
Dipole's arms	rectangle	$l_d = 160$ $w_d = 50$	50
Tapered tips	isosceles triangle	$l_t = 50$	50
Fan-rod	semicircle fans, rectangle rods	$l_f = 410$ $h_f = 105$ $w_f = 100$	50
Gratings	concentric rings	$r_p = 360$	50

nanoampere or higher. Bipolar phototransistors can provide a gain of 2~3 orders of magnitude but suffer from relatively poor frequency response (less than 1 GHz in 3-dB bandwidth). Avalanche photodiodes can offer a better frequency performance (tens of GHz in 3-dB bandwidth) at similar gain but often require high voltage bias and suffer from excess noise from the avanlanche process.

Here, we propose to design a novel core-shell p-n junction nanowire photodetector that can potentially outperform the existing photodetectors in terms of gain and bandwidth. In our design, a small section of the p-type Si nanowire along the axis is partially converted to be n-type by compensation doping, creating a sectional core-shell nanowire similar to a gatelss metal-oxide-semiconductor (MOS) phototransistor, as illustrated in Fig. 3(a). The doping concentration in the core and shell are properly designed to create a weakly depleted channel that is multi-functional. On one hand, the depleted channel suppresses the dark current. On the other hand, since the channel is weakly depeleted, it can be readily turned on by the photogenerated electron-hole pairs, which allows a high concentration of majority carriers to flow across the channel, creating a large gain in photo response.

More specifically, the doping concentrations of the p-type core and n-type shell need to meet the neutral charge constraint, i.e. $n \times w_n = p \times w_p$ where w_n and w_p denote the depletion widths in the n- and p- type parts of the p-n junction, respectively. The weak depletion condition requires w_n and w_p to satisfy $\left(w_n + w_p\right) \le w/2$ and $2w_p \ge w_c$ (Fig. 3(a)) in which w_c is the p-core channel width and w the nanowire width that has been determined in the optical design (height $h = 80nm$ and width $w = 60nm$).

To optimize the design, we tune the p-type background doping concentration from $10^{16}\,cm^{-3}$ to $10^{19}\,cm^{-3}$. For each concentration, the n-type shell doping concentration can be found from the neutral charge constraint discussed above. The optoelectronic simulations are performed after the optical generation results from the finite difference time domain (FDTD) simulation are loaded into the DEVICE module of the Lumerical software in which Newton

#255137 Received 4 Dec 2015; revised 13 Feb 2016; accepted 13 Feb 2016; published 24 Feb 2016

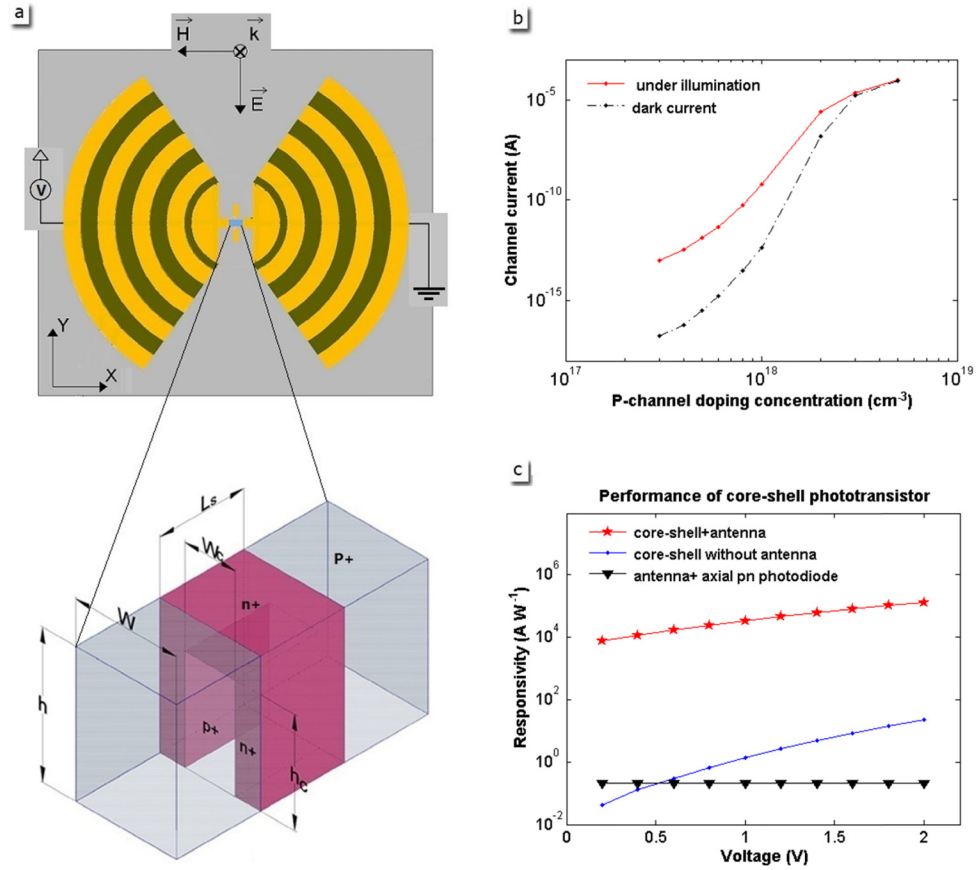

Fig. 3. Design of the core-shell SiNW phototransistor. The n-type shell and p-type core structure makes a weakly depleted p-channel inside the nanogap. (a) Schematic of the device. (b) Photocurrent and dark current of the core-shell SiNW versus p-type background doping concentration. (c) Photoresponsivity of several devices in comparison. Red star line: core-shell nanowire phototransistor integrated with plasmonic antenna. Blue solid-dot line: core-shell nanowire phototransistor without plasmonic antenna. Black triangular line: axial pn junction SiNW photodiode integrated with plasmonic antenna. The incident light intensity is 0.1 $mW\,cm^{-2}$, and the doping concentrations are $n = 1\times10^{19}\ cm^{-3}$ and $p = 1\times10^{18}\ cm^{-3}$.

solver is used for solving Poisson and Drift-Diffusion equations. The dark and photocurrent of the device are plotted in Fig. 3(b) as a function of the p-type background doping concentration under 2 V bias at light intensity of 0.1 $mW\,cm^{-2}$, (close to the light intensity in optical fibers for long distance communication). For designing a high performance photodetector, the rule of thumb is to minimize the dark current and maximize the photocurrent. Unfortunately, the dark and photocurrent of our device both rapidly rise as the background doping concentration increases. Clearly, we need to find a trade-off. A doping concentration of 10^{18} cm^{-3} gives the photocurrent in nano-ampere range and the dark current in sub-pico ampere range. If necessary, the photocurrent can be increased to micro ampere range by tuning the doping concentration, while the dark current still remains orders of magnitude lower. Note that the core channel width is also found to be $w_c = 30\,nm$ at the doping concentration of 10^{18} cm^{-3}. For such a design, to show the optical and electronic gain, we compare the device to the following two devices in photoresponse. The first device is the one without plasmonic antenna (Fig. 3(c), blue solid-dot line). It shows that the plasmonic antenna optically enhances the

#255137 Received 4 Dec 2015; revised 13 Feb 2016; accepted 13 Feb 2016; published 24 Feb 2016

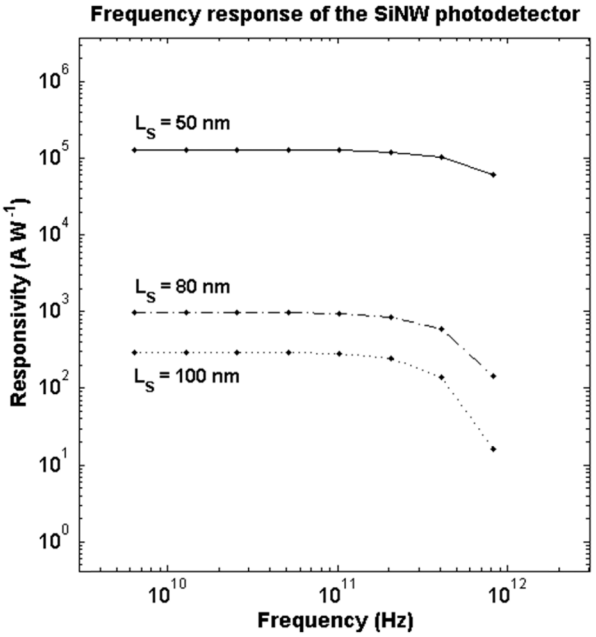

Fig. 4. Frequensy response of SiNW phototransistors. The incident light intensity is $0.1 mW\,cm^{-2}$ and the bias voltage is fixed at 2 V.

photoresponsivity (photocurrent density in the nanowire divided by the incident light intensity) at least 4 orders of magnitude (Fig. 3(c), red star line). The second is the one in which the core-shell phototransistor structure is replaced with a pn junction along the nanowire axis which has no electrical gain (Fig. 3(c), black triangular line). It shows that the core-shell phototransistor enhances the device performance more than 5 orders of magnitude.

It is worthwhile to note that the designed device also shows a robust performance against surface recombination due to the fact that the weakly depleted channel is buried inside the nanowire and mostly away from the surface except the bottom side. In contrast, axial p-n junction devices [18,19] in which the depletion region is exposed to the surface, are far more susceptible to surface recombination and require nearly perfect passivation.

Figure 4 shows the frequency response in photoresponsivity for the device (performed using the commerical device simulator Silvaco). L_s denotes the length of the nanowire core-shell section. Amazingly, the 3dB bandwidth (30% drop in responsivity) for the device with L_s = 50 nm is as high as ~300 GHz. Such an extraordinarily high bandwidth indicates that the carrier transport behavior is unique in our core-shell nanowire phototransistor. Unlike a regular pn junction diode, the photogenerated carriers in our device transport in the radial direction perpendicular to the signal path. The photoucurrent of the device is not directly contributed by the photogenerated carriers. It is instead controlled by the photogating effect, similar to the operating principle of MOS transistors. It is therefore not surprising that a longer sectional length L_s (larger pn junction cross-section) does not result in an increase in photocurrent as observed in the regular pn junction photodiode. The decrease in photocurrent for longer L_s is due to the reduced photogating gain (data not shown here). In MOS transistors, the frequency response is limited by the gate capacitances. Similarly, the frequency performance of our core-shell nanowire device is mainly limited by the time delay associated with the core-shell pn junction. Carrier transport in the axial (signal path) is immediate to maintain charge neutral in the ON channel, and therefore do not contribute the time delay.

#255137 Received 4 Dec 2015; revised 13 Feb 2016; accepted 13 Feb 2016; published 24 Feb 2016

It is known that the time delay of a pn junction includes two parts [20]. The first part is charging/dischaging the space-charge capacitor and the diffusion capacitor. The second part is the transit time that carriers take to transport in radial direction across the depletion region. To provide a rough estimation of the charging/discharging and transit time delays, let us again use the core-shell nanowire phototransistor with L_s = 50 as an exmaple. The junction area of such a device is caculated to be $\sim 160\times 50 nm^2$. Accordingly, the space-charge capacitance (diffusion capacitance can be neglected) is estimated to be as small as $C_j \sim 0.02\, fF$. Considering that both the n and p region are highly doped, the time delay associated with the pn junction capacitance is ~0.28 ps by calculation. The carrier transit time is approximately 0.24 ps (24nm for the depletion region width) if we assume the velocity saturation for electrons (10^7 cm/s). Then the 3dB bandwidth is esitmated to be $f_{3dB} = \frac{1}{2\pi(0.24 ps + 0.28 ps)} = 306 GHz$, which is consistent with the simulation results. In general, a shorter L_s results in a better frequency performance (Fig. 4) due to the reduced junction capacitance, but at the cost of larger dark current (data not shown here). Note that the fringing capacitance of the gratings is not included in the simulations. The 300 GHz bandwidth is the uppper limit of the device performance.

4. Conclusions

In conclusion, we have demonstrated a high-performance SiNW photodetector at communication wavelengths. To turn silicon into a light absorptive material at communication wavelengths, we designed a sophisticated plasmonic antenna structure to increases the intensity of light in the SiNW by 5 orders of magnitude. At the high light intensity, the light absorption in silicon is dominated by the two-photon absorption effect. The generated photocurrent is further amplified by the Si nanowire phototransistor, a section of which is doped to be a core-shell pn junction. Simulation results indicate that the device has achieved a responsivity of 2.4×10^4 A/W and a 3-dB bandwidth over 300 GHz. The designed device structure can be readily applied to other materials such as SiGe to achieve similar or even better performances.

Acknowledgments

This research was financially supported by the national “1000 Young Scholars” program of the Chinese central government, the National Science Foundation of China (NSFC) (No. 61376001), the “Pujiang Talent Program” of the Shanghai municipal government, University of Michigan–Shanghai Jiao Tong University Joint Fund and the Shanghai government foreign student scholarship.

#255137 Received 4 Dec 2015; revised 13 Feb 2016; accepted 13 Feb 2016; published 24 Feb 2016